

Preferential emission into epsilon-near-zero metamaterial [Invited]

Tal Galfsky,^{1,2} Zheng Sun,^{1,2} Zubin Jacob³ and Vinod M. Menon^{1,2,*}

¹Department of Physics, City College of the City University of New York (CUNY) New York, NY, 10031, USA

²Department of Physics, Graduate Center, CUNY, New York, NY, 10016, USA

³Department of Electrical and Computer Engineering, University of Alberta, Edmonton, T6G 2V4, Canada
*vmenon@ccny.cuny.edu

Abstract: We report the use of epsilon near zero (ENZ) metamaterial to control spontaneous emission from Zinc-Oxide (ZnO) excitons. The ENZ material consists of alternating layers of silver and alumina with subwavelength thicknesses, resulting in an effective medium where one of the components of the dielectric constant approach zero between 370nm-440nm wavelength range. Bulk ZnO with photoluminescence maximum in the ENZ regime was deposited via atomic layer deposition to obtain a smooth film with near field coupling to the ENZ metamaterial. Preferential emission from the ZnO layer into the metamaterial with suppression of forward emission by 90% in comparison to ZnO on silicon is observed. We attribute this observation to the presence of dispersionless plasmonic modes in the ENZ regime as shown by the results of theoretical modeling presented here. Integration of ENZ metamaterials with light emitters is an attractive platform for realizing a low threshold subwavelength laser.

©2015 Optical Society of America

OCIS codes: (160.3918) Metamaterials; (160.6000) Semiconductor materials; (300.2140) Emission; (310.4165) Multilayer design; (250.5403) Plasmonics.

References and links

1. B. Edwards, A. Alù, M. E. Young, M. Silveirinha, and N. Engheta, "Experimental Verification of Epsilon-Near-Zero Metamaterial Coupling and Energy Squeezing Using a Microwave Waveguide," *Phys. Rev. Lett.* **100**(3), 033903 (2008).
2. Y. C. Jun, J. Reno, T. Ribauto, E. Shaner, J.-J. Greffet, S. Vassant, F. Marquier, M. Sinclair, and I. Brener, "Epsilon-near-zero strong coupling in metamaterial-semiconductor hybrid structures," *Nano Lett.* **13**(11), 5391–5396 (2013).
3. G. V. Naik, J. Liu, A. V. Kildishev, V. M. Shalaev, and A. Boltasseva, "Demonstration of Al:ZnO as a plasmonic component for near-infrared metamaterials," *Proc. Natl. Acad. Sci. U.S.A.* **109**(23), 8834–8838 (2012).
4. R. Maas, J. Parsons, N. Engheta, and A. Polman, "Experimental realization of an epsilon-near-zero metamaterial at visible wavelengths," *Nat. Photonics* **7**(11), 907–912 (2013).
5. G. Subramania, J. Fischer, and T. S. Luk, "Optical properties of metal-dielectric based epsilon near zero metamaterials," *Appl. Phys. Lett.* **101**(24), 241107 (2012).
6. N. Engheta, "Materials science. Pursuing near-zero response," *Science* **340**(6130), 286–287 (2013).
7. D. C. Adams, S. Inampudi, T. Ribauto, D. Slocum, S. Vangala, N. A. Kuhta, W. D. Goodhue, V. A. Podolskiy, and D. Wasserman, "Funneling Light through a Subwavelength Aperture with Epsilon-Near-Zero Materials," *Phys. Rev. Lett.* **107**(13), 133901 (2011).
8. S. Molesky, C. J. Dewalt, and Z. Jacob, "High temperature epsilon-near-zero and epsilon-near-pole metamaterial emitters for thermophotovoltaics," *Opt. Express* **21**(S1), A96–A110 (2013).
9. P. Ginzburg, F. J. Rodríguez Fortuño, G. A. Wurtz, W. Dickson, A. Murphy, F. Morgan, R. J. Pollard, I. Iorsh, A. Atrashchenko, P. A. Belov, Y. S. Kivshar, A. Nevet, G. Ankonina, M. Orenstein, and A. V. Zayats, "Manipulating polarization of light with ultrathin epsilon-near-zero metamaterials," *Opt. Express* **21**(12), 14907–14917 (2013).
10. A. V. Goncharenko, A. O. Pinchuk, "Broadband epsilon-near-zero composites made of metal nanospheroids," *Opt. Mater. Express* **4**(6), 1276 (2014).
11. C. L. Cortes, W. Newman, S. Molesky, and Z. Jacob, "Quantum nanophotonics using hyperbolic metamaterials," *J. Opt.* **14**(6), 063001 (2012).
12. C. L. Cortes and Z. Jacob, "Photonic analog of a van Hove singularity in metamaterials," *Phys. Rev. B* **88**(4), 045407 (2013).

13. L. Ferrari, D. Lu, D. Lepage, and Z. Liu, "Enhanced spontaneous emission inside hyperbolic metamaterials," *Opt. Express* **22**(4), 4301–4306 (2014).
14. H. N. S. Krishnamoorthy, Z. Jacob, E. Narimanov, I. Kretzschmar, and V. M. Menon, "Topological transitions in metamaterials," *Science* **336**(6078), 205–209 (2012).
15. N. P. Logeeswaran Vj, M. S. Kobayashi, W. Islam, P. Wu, N. X. Chaturvedi, S. Y. Fang, Wang, and R. S. Williams, "Ultrasoother silver thin films deposited with a germanium nucleation layer," *Nano Lett.* **9**(1), 178–182 (2009).
16. W. Chen, K. P. Chen, M. D. Thoreson, V. Kildishev, and V. M. Shalaev, "Ultrathin, ultrasoother, and low-loss silver films via wetting and annealing," *Appl. Phys. Lett.* **97**(21), 211107 (2010).
17. W. D. Newman, C. L. Cortes, and Z. Jacob, "Enhanced and directional single-photon emission in hyperbolic metamaterials," *J. Opt. Soc. Am. B* **30**(4), 766 (2013).
18. D. R. Smith and J. B. Pendry, "Homogenization of metamaterials by field averaging (invited paper)," *J. Opt. Soc. Am. B* **23**(3), 391 (2006).
19. E. M. L. L. D. Landau and L. P. Pitaevskii, *Course of Theoretical Physics*, 2nd, Vol. (Reed, 1984).
20. G. W. Ford and W. H. Weber, "Electromagnetic interactions of molecules with metal surfaces," *Phys. Rep.* **113**(4), 195–287 (1984).
21. T. Baba, "Slow light in photonic crystals," *Nat. Photonics* **2**(8), 465–473 (2008).
22. P. Yao, C. Van Vlack, A. Reza, M. Patterson, M. M. Dignam, and S. Hughes, "Ultrahigh Purcell factors and Lamb shifts in slow-light metamaterial waveguides," *Phys. Rev. B* **80**(19), 195106 (2009).
23. D. Lu, J. J. Kan, E. E. Fullerton, and Z. Liu, "Enhancing spontaneous emission rates of molecules using nanopatterned multilayer hyperbolic metamaterials," *Nat. Nanotechnol.* **9**(1), 48–53 (2014).
24. M. G. Silveirinha, A. Alù, B. Edwards, and N. Engheta, "Overview of theory and applications of epsilon-near-zero materials," *URSI General Assembly* (Chicago, IL, 2008).

1. Introduction

Epsilon near zero (ENZ) metamaterials (MMs) are designed to have one or more components of the dielectric permittivity tensor approach zero for a desired wavelength region. So far ENZ materials have been demonstrated in the micro-wave [1], mid-IR [2,3], and optical regimes [4,5] with applications including super-coupling [6], subwavelength funneling [7], thermophotovoltaic devices [8], and control of spontaneous emission [2].

ENZ metamaterials in the near-UV to near-IR ranges were realized using metal-dielectric composites in nano-rod form [9], nano-spheroids [10], and lamellar multilayers [4,5]. In these structures the zero of the dielectric permittivity can be tuned to a desired range by controlling the fill-fraction of the metal in the structure [11]. One very attractive aspect of this type of MMs is that in the ENZ region light-matter interaction is maximized [12–14]. In this work we have designed a lamellar MM to have an ENZ response for the emission peak of Zinc Oxide (ZnO) and measured the photoluminescence intensity of ZnO grown on top of the structure. We observed an intensity reduction by a factor of ten, in comparison to a reference sample of ZnO grown on silicon (Si) substrate, due to preferential emission into the ENZ MM. This preferential emission is attributed to slow modes governing the photonic density of states (PDOS) in the near zero regime.

2. Design of epsilon near zero metamaterial

The fabricated ENZ metamaterial is a superlattice composed of four periods (4P) of thin alternating layers of alumina (Al_2O_3) and silver (Ag) grown by electron-beam evaporation. For each silver layer an ultra-thin Ge seed layer (1-2nm) was first deposited which ensures the formation of continuous, optically smooth films [15,16]. Figure 1(a) shows a transmission electron microscope (TEM) micrograph of a cross-sectional of the 4P structure displaying the dielectric (D) Al_2O_3 layers and the metallic (M) Ag layers. The thicknesses in nm as determined from the TEM micrograph are from bottom to top; $D_1 = 13$, $M_1 = 16$, $D_2 = 23$, $M_2 = 7.6$, $D_3 = 17.8$, $M_3 = 7.6$, $D_4 = 15$, $M_4 = 7.3$, $D_5(\text{spacer}) = 6.5$. Terminating the MM with a spacer layer is crucial to avoid quenching into a lossy surface plasmon polariton mode [17] The fill fraction of metal in the structure is 0.36 (not including the spacer layer).

We used Effective medium theory (EMT) [18,19] to calculate the permittivity components of the bulk as graphed in Fig. 1(b). The effective medium calculation uses optical constants of thin film Ag and Al_2O_3 that were measured by ellipsometry on samples prepared by electro-beam deposition (see [Data File 1](#) and [Data File 2](#) for the measured optical constants of Ag and Al_2O_3 respectively). In Fig. 1(b) we identify four regions based on the relationship between

the real parts permittivity in the in-plane direction (ϵ_{\parallel}) and the direction perpendicular to the layers (ϵ_{\perp}). In region I where $\epsilon_{\parallel} > 0$, $\epsilon_{\perp} < 0$ the MM has a type I hyperbolic dispersion (the iso-frequency contour forms a discontinuous hyperboloid, see [11]). In region II where both $\epsilon_{\parallel} > 0$, $\epsilon_{\perp} > 0$ the MM has elliptical dispersion and behaves like a lossy anisotropic dielectric material. Region III is the ENZ regime where $\epsilon_{\parallel} \sim 0$, this region overlaps with the emission peak of ZnO at 380nm (marked by vertical dashed line in the figure). In region IV $\epsilon_{\parallel} < 0$, $\epsilon_{\perp} > 0$ and the MM has a type II hyperbolic dispersion (continuous hyperboloid, see [11]). In this work we concentrate on the ENZ regime where light-matter interaction is maximized [14]. We note that on the graph there are also ENZ transitions for ϵ_{\perp} that occur at 325nm and 345nm, however these transitions are sharp so they do not provide a broadband effect and they suffer from more loss than the transition at 400nm for ϵ_{\parallel} . In addition to the effective medium approximation we also employ an exact calculation of the bandstructure of the MM using a dyadic Green function approach [13,20]. The calculation takes into account each layer's thickness as obtained from TEM imaging. The corresponding bandstructure is included in section 5 of this letter.

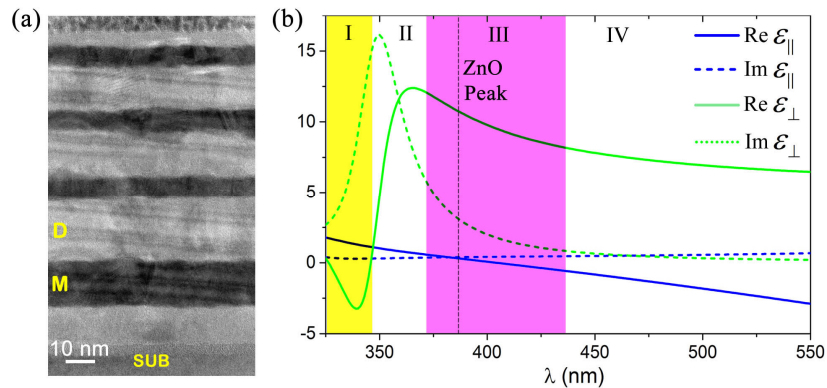


Fig. 1. (a) Cross section of 4P structure imaged by transmission electron microscope (TEM). Ag shows as dark stripes, Al₂O₃ as bright, bottom most layer is Si substrate, topmost layer is a protective Pt layer which is deposited as a part of the cross-sectioning process. (b) Effective permittivity components of the metamaterial. Calculated using optical constants on thin layer Ag and Al₂O₃ obtained from ellipsometry (see [Data File 1](#) and [Data File 2](#)). Region I: Type I hyperbolic dispersion, Region II: Elliptical dispersion, Region III: ENZ regime, Region IV: Type II hyperbolic dispersion. Dashed line marks the emission peak of ZnO.

3. Synthesis of ZnO layers with clean emission spectrum

ZnO was grown by atomic-layer deposition (ALD) on top of the MM. Diethyl zinc (DEZn) and deionized water (H₂O) were used as the source of Zn and O₂, respectively with 0.1s long precursor pulses and the temperature was kept to 85°C. ZnO was deposited on top of the substrate by running a 150 cycles which corresponds to a 15nm layer. Finally, plasma cleaning was executed for 15 minutes to remove oxygen vacancies. The optical quality of the film is highly important for achieving strong, clean emission at room temperatures. To demonstrate this point, Fig. 2(a) shows the photoluminescence (PL) spectrum of ZnO grown on a Si substrate by a different method (electron-beam evaporation). This PL spectrum is dominated by strong emission from surface defects and oxygen vacancies and the ZnO exciton peak at 380nm is completely surpassed by the defects emission. A scanning electron microscope (SEM) image of the sample (Fig. 2(a) inset) shows many surface defects. In contrast ZnO grown by ALD as described above (shown in Fig. 2(b)) exhibits a strong excitonic peak at 380nm with nearly zero emission from defects and an optically flat surface (see SEM image in inset). An AFM surface map of the ZnO layer is graphed in Fig. 2(c) with

a maximum peak to valley roughness of 0.3nm, showing that the ALD grown ZnO is free of surface defects and is indeed optically flat.

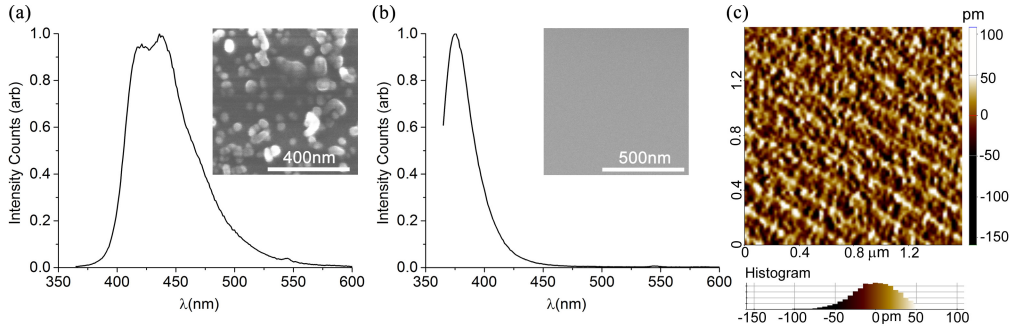


Fig. 2. (a) Photoluminescence (PL) spectrum of electron-beam grown ZnO on Si substrate; inset: SEM image of the sample surface. (b) PL spectrum ZnO grown by ALD. Inset: SEM image of sample surface. (c) Atomic Force Microscope micrograph of the ALD grown sample with a maximum peak to valley roughness of 0.3nm.

4. ZnO emission on ENZ metamaterial

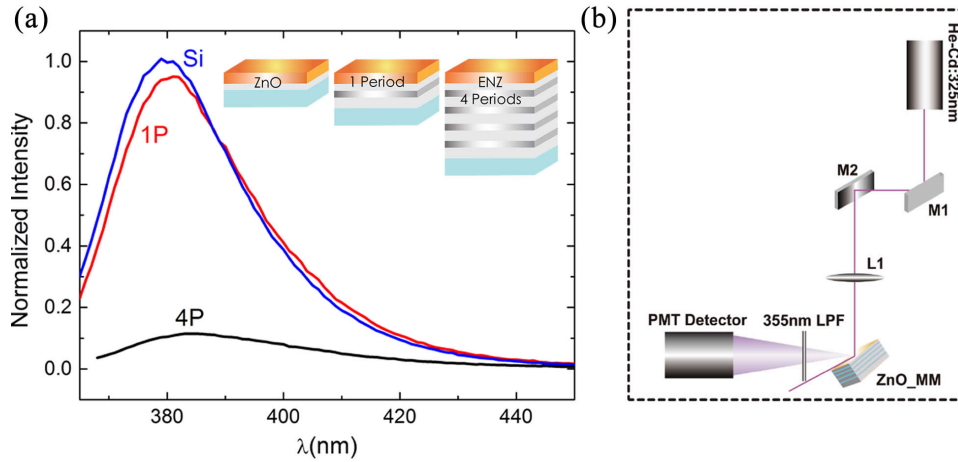


Fig. 3. (a) PL spectrum of ZnO on 4P, 1P, and bare Si, normalized to the PL intensity of ZnO on Si. (b) Schematic of experimental setup for measuring the PL signal.

PL measurements were carried out on an altered Horiba Spectrofluorometer. The samples were pumped by a He-Cd 325nm laser and emission was collected by a photomultiplier tube (PMT) after passing through a 355nm long pass filter (see schematic in Fig. 3(b)). For this measurement 15nm of ZnO were grown on top of Si substrate (reference sample), a control sample consisting of one period (1P) of Al₂O₃/Ge/Ag, and the 4P MM. The ZnO layer was grown in a single process on all the substrates. Figure 4(a) shows the PL intensity for the three samples measured under the same excitation conditions. The inset shows a schematic of the different substrates for ZnO. We measured a 90% reduction in the intensity of emission from the 4P MM in comparison to the 1P reference and control samples. The reason for the fabrication of the 1P reference sample is that in metallic structures the phenomena of quenching is always a concern, therefore a reference sample is needed in order to eliminate to possibility of reduced emission due to quenching into a lossy SPP mode. The amount of quenching into a SPP mode in the 1P and 4P structures is identical since both structures support the same surface mode, however, since the 4P MM also supports bulk modes in addition to the SPP it is expected that radiation would be directed into these modes as

explained in the next section. The dramatic change in emission intensity between 1P and 4P is the indicator of this effect. It should also be noted that the absorption of the pump was ensured to remain the same for all samples.

5. Photonic density of states and EM field simulations

To search for the cause of reduced emission into the far-field from ZnO on top of the 4P structure we calculated the wavelength resolved local photonic density of states (WLDOS) for the ZnO exciton using a dyadic Green function approach [13,20]. In Fig. 4(a) we plot the WLDOS as a function of wavelength and normalized wave-vector, k_x/k_0 . We note that in the ENZ regime the modes in the MM exhibit nearly flat dispersion. As demonstrated in photonic crystals, flat dispersion indicates near zero group velocity [21]. Even in a lossy system the density of states is proportional to the inverse of the group velocity and hence preferential emission into the metamaterial is expected due to light trapping in slow-light modes [12,22].

In addition to the WLDOS calculation, we modeled the exciton emission of ZnO using Finite Element Method with commercial software COMSOL. In the simulation, an exciton is modeled as a perfect electric dipole placed in the middle of a dielectric layer set with the optical constants of ZnO. The layers' thickness and optical constants of the individual layers are taken from the TEM micrograph and from ellipsometry measurements. Figure 4(b) graphs the electric field emitted in the vicinity of the 4P metamaterial for three different wavelengths, corresponding to three regimes of dispersion: Top – Elliptical (at 320nm), Middle – ENZ (at 380nm), Bottom – hyperbolic (at 500nm). See [Visualization 1](#) and [Visualization 2](#) supplementary video files for an emission wavelength scan between 300 and 600nm for horizontal and vertical oriented dipoles respectively. Note that in the two latter cases radiation is enhanced and directed into the metamaterial. For comparison, the inset in middle panel maps the radiation pattern of ZnO on a Si substrate where it is largely reflected to the far-field.

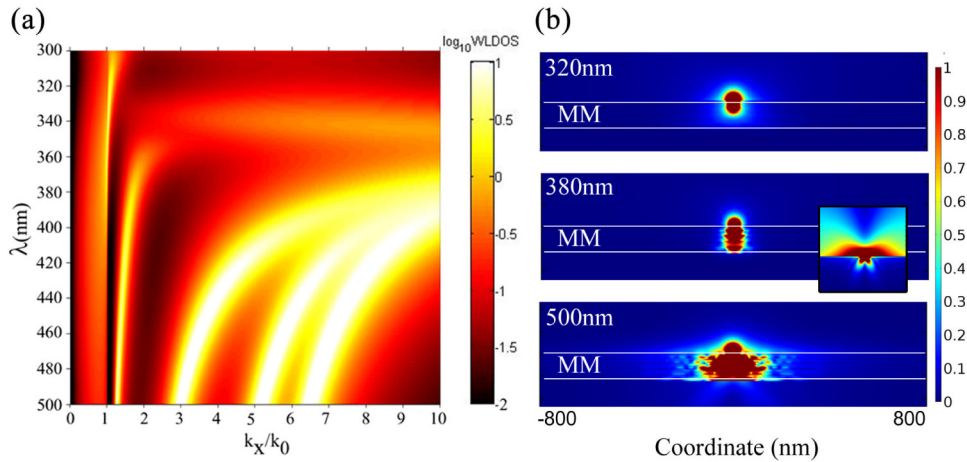


Fig. 4. (a) Wavelength resolved local photonic density of states (WLDOS). The areas where the slope of bright curves begin to flatten are slow modes in the ENZ regime. (b) Simulations of electric field (arb. units) emitted by a dipole embedded in a ZnO layer on top of the 4P metamaterial at three wavelength corresponding to three areas of dispersion, Top: Elliptical (320nm), Middle: ENZ (380nm), Bottom: Hyperbolic (500nm). Inset in middle: radiation of ZnO on Si substrate. See [Visualization 1](#) and [Visualization 2](#) for continuous scan between 300 and 600nm.

6. Discussion

ZnO has large exciton binding energy (~60meV) with bright UV-Blue emission at room temperature and can be grown in a variety of structures including nanorods and nanoparticles. Nanorods can also be used for realizing an ENZ MM in a similar way to what we have shown.

In such a structure, with ZnO embedded as an active component, the enhanced PDOS and the slow modes could possibly be combined to achieve population inversion at lower thresholds. The high anisotropy of the effective permittivity of the MM allows good confinement in one direction and allows directional coupling to a waveguide in the orthogonal direction thus making an ideal on-chip light source. Another very important aspect to consider in these devices is the subject of ohmic loss. As with every plasmonic structure even though the field enhancement factor is large there will be unavoidable ohmic losses as the wave propagates through the material, therefore, the ability to extract the light into a lossless medium is crucial for practical devices. Out-coupling from the ENZ MM can be achieved through nanopatterning or phase matching schemes [2,23,24].

7. Summary

In summary, preferential emission in an ENZ regime has been shown for ZnO on top metal-dielectric superlattice. Preferential emission in EnZ materials can be used for in/out couplers for ultra-subwavelength waveguides and emission into slow modes shows great promise for improving the gain properties of nanoscale plasmonic lasers.

Acknowledgments

We acknowledge support from Army Research Office (W911-NF-15-1-0019), and National Science Foundation (NSF) (DMR-1120923). Research was carried out in part at the Center for Functional Nanomaterials, Brookhaven National Laboratory, which is supported by the U.S. Department of Energy (DOE), Office of Basic Energy Sciences, under Contract No. DE-AC02-98CH10886.